Contribution from the Department of Chemistry and Biochemistry, University of California, Los Angeles, California 90024-1569

Emitting-State Potential Energy Surface and Distortions Calculated from the Excitation Spectrum of Bis(hexafluoroacetylacetonato)platinum(II) in a Molecular Beam

Christian Reber† and Jeffrey I. Zink*

Received December 4, 1991

The excitation spectrum of bis(hexafluoroacetylacetonato)platinum(II), $Pt(hfacac)_2$, is obtained in a supersonic molecular beam. The most intense features in the spectrum are assigned to vibrational structure on the lowest energy ligand to metal charge-transfer band. Effects of the medium on the transition energies are discussed. Progressions in the Pt–O stretch and in ligand modes are observed and compared to low-temperature single-crystal spectra. The intensity distributions are indicative of coupling between normal modes in the excited state. The spectra, the coupling, and the excited state distortions are calculated and interpreted. The major distortion is along the C–O bond of the ligand.

Introduction

Detailed knowledge of geometry changes which occur in molecular excited states has been gained by using a variety of experimental techniques. The most important methods have been absorption, emission, and resonance Raman spectroscopies, either used individually or used in combination.[1] In order to use electronic spectroscopy to measure the distortions along the many normal coordinates which may be displaced, resolution sufficiently high to observe individual vibronic components of the absorption or emission band must be achieved. However, inhomogeneous broadening of spectra obtained in condensed media frequently obscures the desired vibronic bands and only the overall envelope is obtained.

Spectroscopic methods for studying isolated molecules under collision-free conditions in a supersonic molecular beam have recently been developed.[2] Under these conditions, excitation and dispersed luminescence spectra may contain highly resolved vibronic structure even when the molecules are large.[2] Excitation spectra provide the opportunity to study several important aspects of excited electronic states. First, when individual vibronic progressions are resolved, the molecular distortions in the excited state being measured can be calculated. Second, the vibrational frequencies in the excited electronic state can be measured. These measurements complement excited-state Raman and infrared measurements and in addition focus attention on the normal modes which are most strongly affected by the change in bonding properties between the ground and excited states. Third, the spectra of the isolated molecules in the gas phase can be compared with spectra in condensed media and the effects of solvent or crystal packing can be quantitatively determined. Finally, when high resolution is obtained, detailed information about the ground and excited state potential surfaces can be extracted. Of particular interest is the possibility of determining deviations from harmonic oscillator behavior and of the existence of coupling between normal modes.

In this paper, we report the first spectrum of a transition metal coordination compound bis(hexafluoroacetylacetonato)platinum(II), $Pt(hfacac)_2$, in a supersonic molecular beam. Attention is focused on the lowest ligand to metal charge-transfer band. The electronic excited states and the vibronic components are assigned. The differences between the beam spectrum and the spectra obtained in condensed media are discussed. The excited-state geometry is calculated. Detailed aspects of the excited-state potential surface, especially coupling between normal modes, are quantitatively analyzed.

Experimental Section

The excitation spectra of $Pt(hfacac)_2$ were measured in a stainless steel vacuum chamber (cubic, edge length 30 cm). A roughing pump (E2M18, 25 $m^3\ h^{-1}$) and a diffusion pump (Varian, 12-in. diameter, connected directly to the vacuum chamber) were used to evacuate the chamber. Pressures of $\sim 8 \times 10^{-5}$ and 7×10^{-6} Torr were routinely achieved with and without the molecular beam, respectively. The $Pt(hfacac)_2$ molecules in a stream of Ar carrier gas were expanded adiabatically through a nozzle (100-μm diameter, Ealing pinhole) into the vacuum chamber to generate the collision-free supersonic molecular beam. Temperatures on the order of 10 K were determined for large organic molecules such as quinizarin in our apparatus.[3] No temperature could be determined for $Pt(hfacac)_2$, but we assume it to be similar to that of the organic molecules. The $Pt(hfacac)_2$ complexes in the molecular beam were excited with a dye laser (Lambda Physik FL 2001) pumped by an excimer laser (Lambda Physik MSC 201, operated at 30 Hz). The line width of the dye laser was less than 0.1 Å in all the experiments, less by almost 2 orders of magnitude than the line widths measured in the excitation spectrum. Pulse energies were 1–2 mJ at the maximum of the gain profile of the laser dye. The excitation spectra were taken at wavelength intervals of 0.05–0.1 Å. The laser beam crossed the molecular beam at an angle of 90°. The emitted light was collected by a photomultiplier (Hamamatsu R928) positioned at an angle of 90° to both the laser and molecular beams. Scattered excitation light was cut off by appropriate filters. A series of different filters were used with every laser dye in order to exclude filter artifacts in the spectrum. The detector signal was averaged with a boxcar averager (Stanford Research SR 250, input terminator, 1 kΩ) using a gate width of 1 μs and a delay time of 100 ns after the pulse to minimize the signal from the scattered excitation light. In a typical experiment, 300 laser pulses were averaged to measure one point in the excitation spectrum. The output power of the dye laser was recorded with a photodiode and averaged with a transient digitizer (Sony/Tektronix RTD710) over the same number of pulses as the signal from the photomultiplier. The dye laser wavelength and the averaged signals from both the photomultiplier and the photodiode were stored on a microcomputer. The boxcar averager, the transient digitizer, and the dye laser wavelength were computer controlled.

The data processing consisted of three steps. In the first step, the experimental raw data, i.e. intensities vs excitation wavelength from both detectors, were plotted in order to check the dye laser output power against the literature gain curve and, by comparison with the signal from the molecular beam recorded with the photomultiplier tube, to qualitatively locate peak positions and intensities of molecular transitions from $Pt(hfacac)_2$. In the second step, the signal obtained from the photomultiplier was divided by the laser intensity, yielding the excitation spectrum corrected for the dye laser output power. In the final step, the intensities in the overlapping wavelength range of the dyes were matched. The spectrum shown in Figure 1 required eight dyes and therefore seven such matches. Although the portion of the total spectrum obtained with every laser dye was reproduced at least three times, the intensity-matching procedure introduces an uncertainty in the peak intensities throughout the spectrum which is larger than that in an excitation spectrum over the same wavelength range recorded with a conventional scanning instrument.

$Pt(hfacac)_2$ was used as obtained from Strem Chemicals Inc. Sublimation of the compound did not change the spectra. The vapor pressure of $Pt(hfacac)_2$ at 100 °C is ca. 1 Torr.[4] The sample compartment in the vacuum chamber was heated to 100 °C, and Ar gas with a backing pressure of 100 mbar was used as a carrier.

† Current address: Department of Chemistry, University of Montreal, Montreal H3C 3J7, Canada.

(1) Zink, J. I.; Shin, K. S. *Molecular Distortions in Excited Electronic States Determined from Electronic and Resonance Raman Spectroscopy*; Advances in Photochemistry, Vol. 16; Wiley: New York, 1991; pp 119–214.
(2) Smalley, R. E.; Wharton, L.; Levy, D. H. *Acc. Chem. Res.* **1977**, *10*, 139.
(3) Subbi, J. *Chem. Phys. Lett.* **1984**, *1*, 109.
(4) Wolf, W. R.; Sievers, R. E.; Brown, G. H. *Inorg. Chem.* **1972**, *11*, 1995.

0020-1669/92/1331-2786$03.00/0

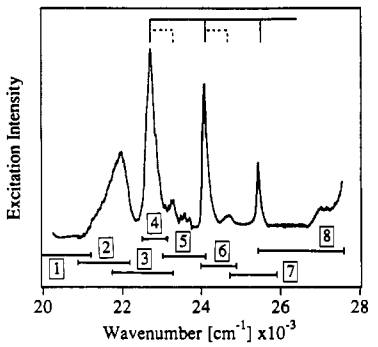

Figure 1. Excitation spectrum of $Pt(hfacac)_2$ in a molecular beam. The solid and dotted lines on top of the spectrum indicate the progressions in the 1350- and 597-cm^{-1} modes, respectively. The wavenumber regions of the dyes used to obtain the spectrum are shown below the spectrum. The dyes are (1) Coumarin 480, (2) Coumarin 460, (3) Coumarin 440, (4) POPOP, (5) Bis-MSB, (6) DPS, (7) α-NPO, and (8) BBQ. The wavenumber regions of the dyes used to obtain the spectrum are shown.

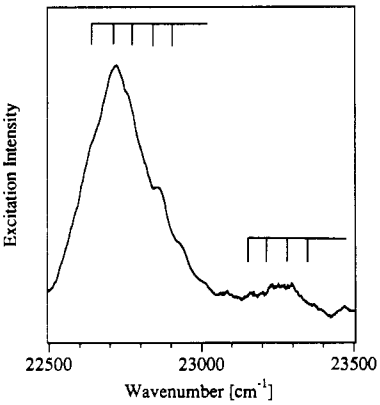

Figure 2. Expanded view of the excitation spectrum of $Pt(hfacac)_2$ in a molecular beam in the region between 22 500 and 23 500 cm^{-1}. The progression in the 65-cm^{-1} mode is indicated on the top.

The experimental setups used for the measurement of the single-crystal luminescence and absorption spectra have been described previously.[5]

Results

A. Excitation Spectrum in the Beam. The excitation spectrum of $Pt(hfacac)_2$ in the supersonic molecular beam is shown in Figure 1. Strong signals were recorded between 22 000 and 26 000 cm^{-1}. The dyes which were used to span this relatively large range and the specific regions accessible with the individual dyes are also shown. The lowest energy feature is a broad band with very little resolved structure. Its onset occurs at about 21 000 cm^{-1}, and its maximum is at 21 900 cm^{-1}. The higher energy region of the spectrum is dominated by a set of three sharper bands with maxima at 22 700, 23 985, and 25 400 cm^{-1}. These bands, with an average separation of 1350 cm^{-1}, contain resolvable fine structure. Finally, smaller features containing fine structure are observed between the three sharp, intense bands.

The magnified spectrum in the region between 22 500 and 23 500 cm^{-1} containing the first of the intense, sharp bands as well as some of the smaller features is shown in Figure 2. The vibronic fine structure on the most intense band is evident in the expanded spectrum. These vibronic bands are not well resolved, but a regular spacing between the shoulders of 65 cm^{-1} is found. The vibronic structure in the least intense band in Figure 2 is even less well resolved, but the same energy spacing is evident.

A partial list of the band energies, organized in a manner appropriate for the following discussion, is given in Table I. The three most important energy spacings are the 1350-cm^{-1} separation between the sharp, intense features, the 597-cm^{-1} separation between the sharp features and the first peak to the higher energy side of the sharp features, and the 65-cm^{-1} average separation between the shoulders on these peaks.

(5) Tutt, L. W.; Zink, J. I. *J. Am. Chem. Soc.* **1986**, *108*, 5830. Chang, T. H.; Zink, J. I. *J. Am. Chem. Soc.* **1984**, *106*, 287.

Table I. Selected Transition Energies and Assignments for the Excitation Spectra of $Pt(hfacac)_2$ in a Molecular Beam[a]

no.	transn energy, cm^{-1}	assignt	no.	transn energy, cm^{-1}	assignt
1	22 613	electronic origin	7	23 985	(1) + $\hbar\omega_{CO}$
2	22 700	(1) + $\hbar\omega_{lig}$	8	24 055	(7) + $\hbar\omega_{lig}$
3	22 771	(1) + $2\hbar\omega_{lig}$	9	24 120	(7) + $2\hbar\omega_{lig}$
4	22 843	(1) + $3\hbar\omega_{lig}$	10	24 645	(7) + $\hbar\omega_{PtO}$
5	22 921	(1) + $4\hbar\omega_{lig}$	11	25 400	(1) + $2\hbar\omega_{CO}$
6	23 220	(1) + $\hbar\omega_{PtO}$	12	25 455	(11) + $\hbar\omega_{lig}$

[a] Assignments refer to the numbers in the left-hand column.

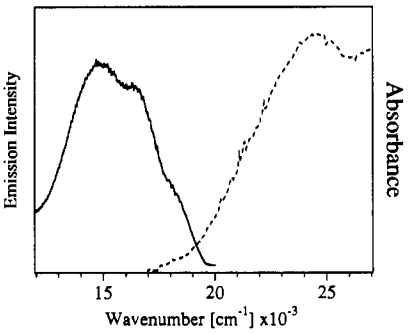

Figure 3. Single-crystal luminescence spectrum at 20 K (solid line) and absorption spectrum at 77 K (dashed line). The luminescence was excited at 364 nm.

Attempts to record the dispersed emission spectrum while the molecule was excited in the 22 000–24 000-cm^{-1} region were unsuccessful although emission spectra of organic molecules in the molecular beam could be measured in our apparatus. The large wavelength range covered by the spectrum, the relatively broad vibronic structure, and relaxation processes between excited states close in energy could cause the dispersed emission signal at every element of the diode array (EG&G OMA III) to be below the detection limit.

B. Spectra of the Molecule in Condensed Media. The absorption spectrum of a single crystal of $Pt(hfacac)_2$ at 77 K is shown on the right-hand side of Figure 3. A broad peak with a maximum at 25 000 cm^{-1} and a width at half-height of 4000 cm^{-1} is observed. This broad band spans the same energy region as the three dominant bands in the molecular beam excitation spectrum. The crystal absorption spectrum contains almost no vibronic fine structure.

The absorption spectrum in cyclohexane solution at room temperature also contains a broad band at about 23 000 cm^{-1} with a molar absorptivity of $>10^3$ M^{-1} cm^{-1}. This band contains poorly resolved vibronic bands at about 22 010, 23 100, and 24 200 cm^{-1}. A weaker band is found to low energy at 22 000 cm^{-1}.

The single-crystal emission spectrum of $Pt(hfacac)_2$ at 77 K is shown on the left side of Figure 3. The bandwidth of 4000 cm^{-1} is about the same as that of the single-crystal absorption band. The onset of the emission band overlaps that of the absorption band at about 19 000 cm^{-1}. Poorly resolved vibronic fine structure is observed with an energy spacing of 1400 cm^{-1}.

Discussion

A. Assignments of the Excitation Bands. The bands observed in the excitation spectrum of $Pt(hfacac)_2$ in the molecular beam are assigned to transitions to two electronic states: a low-lying ligand field excited state and a slightly higher energy ligand to metal charge-transfer (LMCT) excited state. The band with its peak maximum at 21 900 cm^{-1} and weak features to higher energy are assigned to the ligand field excited state. The weak features arise from vibronic structure. The prominent series of sharp intense bands at 22 700, 23 985, and 25 400 cm^{-1} are assigned to vibronic components of the LMCT state. The weak bands 597

cm^{-1} to higher energy from each of these bands are assigned to additional vibronic components of the LMCT state. The bases of these assignments are the molar absorptivities[6-9] and previously reported photoelectron spectroscopic results and molecular orbital calculations.[10,11]

The major experimental basis for assigning the bands to ligand field and charge-transfer transitions is the molar absorptivity measured in the solution spectrum. The lowest energy band observed in the solution spectrum has a molar absorptivity on the order of 10^2 M^{-1} cm^{-1}. This value is typical for spin-allowed ligand field transitions in square planar platinum(II) complexes.[6-9] The next higher energy band in the solution spectrum at 23 000 cm^{-1} has a molar absorptivity of $>10^3$ M^{-1} cm^{-1} which is typical for a charge-transfer transition. Similar bands, a weak feature at about 20 000 cm^{-1} and a stronger feature at 25 000 cm^{-1}, have been reported in the absorption spectrum obtained from a hot gas.[12] (The spectrum was given as the transmission spectrum, and no molar absorptivities were reported.)

The assignment of the intense band in the beam spectrum to a LMCT transfer is supported by molecular orbital calculations.[10] Pseudopotential ab initio calculations indicated that the highest occupied molecular orbital in $Pt(acac)_2$ is mainly ligand π antibonding in character. The results of the calculation compared well with photelectron spectroscopic data.[11] Because the absorption spectrum of the acac complex is very similar to that of the hfacac complex investigated here, it is reasonable to assume that the assignments are the same for both complexes. Thus, the intense band arises from a transition from the π ligand orbital to either an orbital primarily metal d in character (LMCT) or an orbital mainly ligand π antibonding in character (ligand π–π^*). Previous studies have shown that the ligand-centered π–π^* transition in acac complexes occurs at higher energies in the region of 35 000 cm^{-1}.[13] We thus assign the state at about 24 000 cm^{-1} to LMCT.

B. Effect of the Medium on the Band Energies. The measurement of the LMCT-state energy from isolated molecules in the gas phase enables comparisons to be made between the gas phase and condensed media. The LMCT band observed from isolated molecules in the molecular beam excitation spectrum is blue shifted relative to the absorption bands obtained in condensed media. When the environment is changed from cyclohexane to the beam, a blue shift of the first vibronic peak of 600 cm^{-1} is observed. This shift is measured from the center of the first shoulder in the solution spectrum and the center of the 22 700–cm^{-1} peak in the beam spectrum. The shift is small but it is significant, especially since cyclohexane is often assumed to have very weak effects on the spectra of solutes because it is a nonpolar, noncoordinating solvent.

The shift of the LMCT band when the medium is changed from the crystal to the molecular beam is much larger. It is estimated to be larger than 1000 cm^{-1}. A more accurate measurement is impossible because the crystal spectrum is broad and unstructured. The shift is estimated from the difference in energy between the peak maximum in the broad crystal spectrum and the weighted center of the well-resolved vibronic bands in the beam spectrum.

The relative energies of the ligand field and the LMCT states change as a function of the medium of the molecule. In isolated molecules in the molecular beam, the lowest energy band is assigned as a ligand field transition. The ligand field band is also lowest in energy in the hot gas spectrum and in the cyclohexane solution spectrum. On the other hand, the lowest energy band in the crystal is the LMCT band. This is evident from the single-crystal spectra in Figure 3. The identical widths of the absorption and emission bands indicate that the LMCT state is the emitting state. The width of an emission band from the ligand field state would be expected to be less than 2000 cm^{-1}, similar to the width of the d–d absorption band observed in hexane solution, in the hot gas[12] and in the molecular beam. A possible explanation for the observed band energy changes is the change in the energy of the ligand field excited state as a function of axial interactions. In the crystal, axial interactions with other molecules raise the energy of the ligand field band higher than that of the LMCT band. In the gas phase and in the poorly coordinating solvent, axial interactions are weak and the ligand field band lies lower than the LMCT state. In addition, the LMCT state blue-shifts by more than 1000 cm^{-1} from condensed media to the gas phase. Both of these effects combine to give the observed energy ordering of the states.

C. Assignment of the Vibronic Structure. The vibronic peaks in the molecular beam excitation spectrum are assigned by comparison with the electronic-ground-state vibrations of the molecule and of analagous bis(acetylacetonato) complexes. The three prominent peaks separated by 1350 cm^{-1} are assigned to a progression in the totally symmetric CO stretching mode. The 1603-cm^{-1} mode in the Raman spectrum of $Pt(hfacac)_2$ and the 1565-cm^{-1} mode of $Pt(acac)_2$ arise from the totally symmetric CO stretch.[14] This mode is observed between 1520 and 1600 cm^{-1} in a variety of divalent transition metal acetylacetonato complexes.[15] The decreased frequency in the excited electronic state relative to that in the ground state is expected due to the reduced CO bond order in the emitting state.

The small peaks that are found 597 cm^{-1} to higher energy from the sharp peaks in the molecular beam spectrum are assigned to a quantum of the PtO totally symmetric stretch. In the Raman spectra of $Pt(hfacac)_2$ and $Pt(acac)_2$, the PtO stretch occurs at 635 and 485 cm^{-1}, respectively.[14] It occurs between 420 and 500 cm^{-1} in a series of metal acetylacetonate complexes.[15] The band in the 23 000-cm^{-1} region of the molecular beam spectrum is overlapped by components of the ligand field band.

The structure on the above peaks with a separation of 65 cm^{-1} arises from a progression in a totally symmetric ring deformation mode. Low-frequency modes in the 100–200-cm^{-1} range of the IR spectrum of $Pt(hfacac)_2$ and $Pt(acac)_2$ have been observed and attributed to ring deformation modes but not completely assigned.[15,16]

The spacings corresponding to the above assignments are shown in Figures 1 and 2. The LMCT spectrum is dominated by progressions in these three modes. Distortions in these modes are expected in a transition which involves the π system on the ligand and a metal d orbital involved in Pt–O bonding. The magnitudes of the distortion and the intensity of specific features of the vibronic structure are analyzed in the following sections.

D. Normal-Mode Coupling and Calculation of the Excitation Spectrum. In this section the intensities of the vibronic transitions in Figure 1 are quantitatively analyzed in order to obtain a detailed excited-state potential surface and to calculate the excited-state geometry. We focus on the ligand to metal charge-transfer transition in the 22 500–26 000-cm^{-1} region. Time-dependent theory is used to calculate the spectrum from the multidimensional potential surfaces of the initial and final states.[17,18] For isolated molecules in the gas phase, the excitation spectrum is identical to the absorption spectrum. The excitation intensity $I(\omega)$ as a function of the wavenumber ω is given by

$$I(\omega) = C\omega \int_{-\infty}^{+\infty} \exp(i\omega t)\left[\langle \phi\phi(t)\rangle \exp\left(-\Gamma^2 t^2 + \frac{iE_0}{\hbar}t\right)\right] dt \quad (1)$$

(6) Chang, T. H.; Zink, J. I. *Inorg. Chem.* **1985**, *24*, 4499.
(7) Chang, T. H.; Zink, J. I. *Inorg. Chem.* **1986**, *25*, 2736.
(8) Fanwick, P. E.; Martin, D. S. *Inorg. Chem.* **1973**, *12*, 24.
(9) Jorgensen, C. K. *Absorption Spectra and Chemical Bonding in Complexes*; Pergamon Press: Oxford, U. K., 1962, Chapter 6.
(10) Di Bella, D.; Fragala, I.; Granozzi, G. *Inorg. Chem.* **1986**, *25*, 3997.
(11) Fragala, I.; Costanzo, L. L.; Ciliberto, E.; Condorelli, G.; D'Arrigo, C. *Inorg. Chim. Acta* **1980**, *40*, 15.
(12) Mingxin, Q.; Nonot, R.; van den Bergh, H. *Sci. Sin. Ser. B (Engl. Ed.)* **1984**, 531.
(13) Lintvedt, R. L.; Kernitsky, K. K. *Inorg. Chem.* **1970**, *9*, 491.
(14) Kradenov, K. V.; Kolesov, B. A.; Zharkova, G. I.; Isakova, V. G. *Zh. Strukt. Khim.* 1988, *31*, 56.
(15) Nakamoto, K.; McCarthy, P. J.; Martell, A. *J. Am. Chem. Soc.* **1961**, *83*, 1272.
(16) Oglezneva, I. M.; Igumenov, I. K. *Koord. Khim.* **1984**, *10*, 313.
(17) Heller, E. J. *Acc. Chem. Res.* **1981**, *14*, 368.
(18) Heller, E. J. *J. Chem. Phys.* **1978**, *68*, 2066.

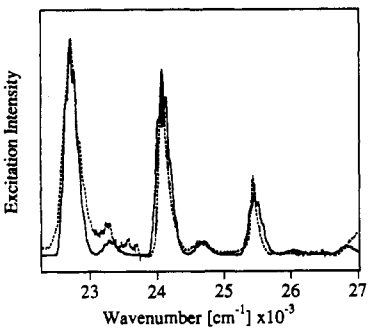

Figure 4. Calculated (solid line) and experimental (dotted line) excitation spectra. The calculated spectrum is the best fit obtained by using an uncoupled harmonic potential surface (eq 4).

ϕ is the ground-state vibrational eigenfunction of the ground electronic state of the molecule. It is assumed to be a Gaussian (the lowest energy eigenfunction of a harmonic potential) in all of our calculations. ϕ is displaced vertically to the excited-state potential surface and evolves there with time. The autocorrelation function $\langle\phi\phi(t)\rangle$ is Fourier-transformed according to eq 1 to yield the spectrum. Γ is a phenomenological damping factor obtained from the experimental line width, and E_0 is the energy of the electronic origin transition. For uncoupled coordinates, the total autocorrelation function $\langle\phi\phi(t)\rangle$ in eq 1 is the product of the autocorrelation along every coordinate.

$$\langle\phi\phi(t)\rangle = \prod_k \langle\phi_k|\phi_k(t)\rangle \qquad (2)$$

The assumption of uncoupled coordinates reduces the computer time by at least an order of magnitude, because only one-dimensional wave functions need to be calculated and propagated. However, as shown below, uncoupled coordinates cannot account for the vibronic intensities in the experimental spectrum and coupling must be included.

In order to calculate $\phi(t)$ from $\phi(t=0)$, the split-operator method of Kosloff, Feit, and Fleck[19,20] is used.

$$\phi(t+\Delta t) = \left[\exp\left(\left(\frac{i\Delta t}{4M}\right)\nabla^2\right)\right][\exp(-i(\Delta t)V)] \times \left[\exp\left(\left(\frac{i\Delta t}{4M}\right)\nabla^2\right)\right]\phi(t) + O[(\Delta t)^3] \qquad (3)$$

Starting with $\phi(t=0)$, the evolution of ϕ with time can be calculated to high accuracy. V denotes the excited-state potential. The most important components that determine V are the excited-state distortions, i.e. the position of the potential minimum along the configurational coordinates of the vibrational modes involved. Only modes with a displacement in the excited state contribute to vibronic structure in an allowed transition, and therefore only these modes need to be considered in our calculation.

The modes involved in the vibronic structure of the LMCT transition of $Pt(hfacac)_2$ are the C–O stretching, the Pt–O stretching, and a ligand ring bending vibration. The simplest trial potential V is harmonic along the configurational coordinates Q of all three modes:

$$V = V_{harm} = \tfrac{1}{2}[k_{CO}(Q_{CO} + \Delta C_O)^2 + k_{PtO}(Q_{PtO} + \Delta_{PtO})^2 + k_{lig}(Q_{lig} + \Delta_{lig})^2] \qquad (4)$$

Both Q_i and Δ_i are in dimensionless units, and therefore the force constants k_i are equal to the excited-state vibrational energies in wavenumbers. The latter are obtained from the spectrum (Figure 1 and Table I). The Δ_i denote the excited-state distortions and are the parameters to be determined. The values of both E_0 (22 613 cm^{-1}) and Γ (19 cm^{-1}) are obtained from the spectrum in Figure 1. The initial wavepacket ϕ is calculated by using the literature values for the ground-state vibrational energies along the three modes.

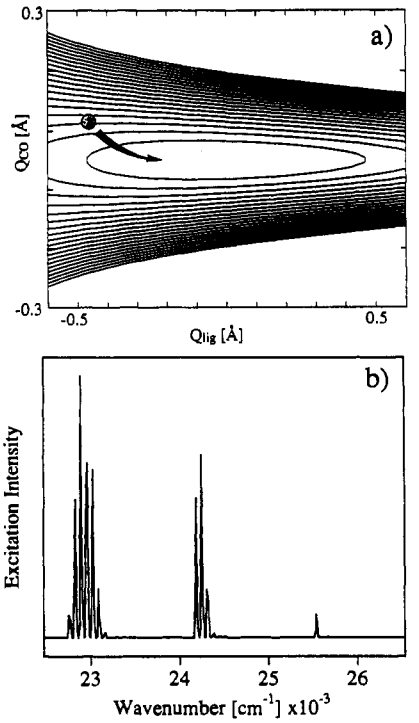

Figure 5. Top: Excited-state potential surface illustrating coupling between the 1350- and 100-cm^{-1} normal modes. The potential surface was calculated by using eq 5. The starting position of the wavepacket is shown by the dot. Bottom: Excitation spectrum calculated by using this surface. The decrease in bandwidth of the 1350-cm^{-1} progression with increasing wavenumber is shown.

The best fit spectrum calculated by using the harmonic, uncoupled potential is compared to the experiment in Figure 4. The overall agreement is good in view of the simplicity of the model. The main progression in the 1350-cm^{-1} mode with its low-energy fine structure is well reproduced. The intensity of the first sideband in the 597-cm^{-1} mode at 23 220 cm^{-1} cannot be determined accurately from the experimental spectrum due to the overlap with the low-energy d–d band. The values of Δ obtained from the calculations are $\Delta_{CO} = 1.18$, $\Delta_{PtO} = 0.48$, and $\Delta_{lig} = 2.18$.

The major discrepancy between the experimental and calculated LMCT spectra of Figure 4 involves the widths of the transitions forming the 1350-cm^{-1} progression. The experimental widths are 326, 152, and 102 cm^{-1} for the bands in order of increasing energy. These widths are governed by the progression in the 65-cm^{-1} ligand ring bending mode, which is superimposed on every member of the 1350-cm^{-1} progression in the C–O stretching vibration. The uncoupled harmonic calculation in Figure 4 gives a *constant* width of 202 cm^{-1} for all the members of the main progression. The uncoupled potential surface model is therefore not able to account for the observed trend in these widths. The changes in the widths are evidence for coupling between the normal coordinates in the excited state.

The simplest form of coupling is

$$V = V_{harm} + c(Q_{lig}Q_{CO}^2) \qquad (5)$$

where V_{harm} is given in eq 4 and the second term is the coupling between the two modes governing the experimental widths. This coupled potential surface includes the coupling constant c as an adjustable parameter. It is shown for $c = 0.25$ in Figure 5a. The time evolution of the wavepacket ϕ on this surface is no longer independent along Q_{CO} and Q_{lig}, and therefore a calculation on the full two-dimensional surface is needed for the two coupled modes. Equation 2 can no longer be applied to this situation. Because no experimental evidence of coupling is observed for the Pt–O stretching mode, its autocorrelation is calculated independently and multiplied to the autocorrelation for the two coupled modes to obtain the full spectrum.

(19) Kosloff, D.; Kosloff, R. *J. Comput. Phys.* **1983**, *52*, 35.
(20) Feit, M. D.; Fleck, J. A.; Steiger, A. *J. Comput. Phys.* **1982**, *47*, 412. (For an introductory overview see: Tanner, J. J. *J. Chem. Educ.* **1990**, *67*, 917.)

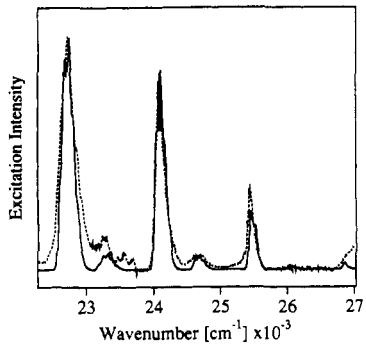

Figure 6. Comparison of the experimental spectrum (dotted line) with that calculated by using the excited-state potential surface defined in eq 5 with coupling between the two modes (solid line), as described in section D. The bandwidths are fit more accurately than by the uncoupled potential surface used to calculate Figure 4.

The excitation spectrum calculated with the two-dimensional potential surface in Figure 5a is shown in Figure 5b. The starting position of the moving wavepacket is shown as a black dot in Figure 5a. The calculated spectrum in Figure 5b shows the pronounced effects of the coupling: the widths of the bands constituting the main progression decrease dramatically with increasing transition energy and show the same trend as that observed in the experiment. In this pedagogical calculation, a value of 5 cm^{-1} was chosen for Γ in order to clearly illustrate the changes in the low-energy progression on the three peaks separated by 1350 cm^{-1}. The varying width of the low-frequency structure on the members of a high-frequency progression can be explained from the time-dependent viewpoint. The initial wavepacket starts to evolve along the steepest gradient on the potential surface in Figure 5a toward the potential minimum. At every point of its trajectory, it encounters a different shape of the potential along the Q_{lig} coordinate, depending on its position along Q_{CO}. This change in the shape of the potential leads to the change of the intensity distribution in the low-frequency progression on every member of the main progression in Figure 5b. For the situation in Figure 5 and in the spectrum in Figure 1, where three members of the high-energy progression are observable, the widths decrease if the wavepacket starts on the shallow side of the coupled potential and increase if the wavepacket starts on the steep side of the coupled potential. (These simple trends do not hold for longer progressions. A more detailed analysis of analogous situations will be published elsewhere.[21])

The calculated spectrum with the coupled harmonic excited-state potential (eq 5) is compared to the experimental spectrum in Figure 6. The agreement between the calculation and the experiment is significantly better than with the uncoupled harmonic potential (eq 4). The observed trend of decreasing width of the members of the main progression is reproduced by starting the wavepacket on the shallow side of the potential as illustrated in Figure 5. The remaining small discrepancies are most likely due to the simple functional form of the coupling term and the limitation of the coupling to only two of the three vibrational modes. The values of the parameters for the coupled harmonic potential (eq 5) are $\Delta_{CO} = 1.04$ (−11% change from the uncoupled model), $\Delta_{lig} = 2.16$ (−1% change), $\Delta_{PtO} = 0.48$ (unchanged), and $c = 0.11$. The best fit values of Δ obtained with the coupled and uncoupled potential surfaces are therefore very similar, although the effect of coupling on the spectrum is pronounced.

E. Excited-State Geometry. The values of Δ obtained by fitting the calculated spectrum to the experimental spectrum determine the minimum of the potential surface in configuration coordinate space and hence the bond length and bond angle changes which occur when the molecule is excited. In order to convert the dimensionless distortions into bond length and bond angle changes, a full normal-coordinate analysis is required. Because such an analysis has not been completed, a few simple assumptions will

(21) Wexler, D.; Zink, J. I. Manuscript in preparation.

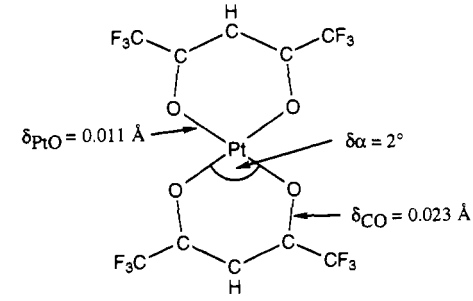

Figure 7. Excited-state distortions of Pt(hfacac)$_2$ in the molecular beam.

be used to give an estimate of the distortions. For both stretching vibrations, the mass was assumed to be 16 g/mol, and for the ligand ring bending mode it was assumed to be 28 g/mol (one CO fragment). The relationships between the bond length changes δ_i, the bond angle changes $\delta\alpha_1$, and the normal coordinates ΔQ_i are approximated to be

$$\Delta Q_{CO} = \tfrac{1}{2}(\delta_{CO1} + \delta_{CO2} + \delta_{CO3} + \delta_{CO4}) \quad (6)$$

$$\Delta Q_{PtO} = \tfrac{1}{2}(\delta_{PtO1} + \delta_{PtO2} + \delta_{PtO3} + \delta_{PtO4}) \quad (7)$$

$$\Delta Q_{lig} = \tfrac{1}{2}(\delta\alpha_{(CO-Pt-CO)1} + \delta\alpha_{(CO-Pt-CO)2} + \delta\alpha_{(CO-C-CO)1} + \delta\alpha_{(CO-C-CO)2}) \quad (8)$$

The numerical values obtained from eqs 6–8 and Δ's obtained from the fit using the coupled potential are $\delta_{CO} = 0.023$ Å, $\delta_{PtO} = 0.011$ Å, and $\delta\alpha = 2.0°$.[22] The values obtained by using the uncoupled potentials are $\delta_{CO} = 0.021$ Å, $\delta_{PtO} = 0.011$ Å, and $\delta\alpha = 2.0°$. The differences between the distortions calculated with the coupled and uncoupled models are very small, probably smaller than the uncertainties introduced by using the approximations of eqs 6–8 for the normal coordinates. The excited-state structure of Pt(hfacac)$_2$ determined from the excitation spectrum in the molecular beam is shown schematically in Figure 7.

Two aspects of the distortions deserve further comment. First, it is surprising that the distortions calculated by using the coupled potential surface differ only slightly from those calculated by using the simple uncoupled-surface model. The coupling which is involved is small, but it causes obvious changes in the spectrum. The changing widths in the jet spectrum clearly show that coupling occurs. However, even the simple model provides a very good estimate of the excited-state geometry. Second, the distortions that occur are those which are expected in a LMCT transition. The major changes are expected to be in the metal–ligand Pt–O bond and in the C–O and C–C bonds in the ring, as are observed. The largest change occurs in the C–O bond on the ligand.

For this molecule, the almost featureless crystal spectra do not allow such a detailed analysis of the excited-state geometry and potential surface to be made. Excitation spectroscopy in a molecular beam is a powerful technique leading to more insight into the excited-state properties of transition metal compounds.

Acknowledgment. We thank Dr. Juhan Subbi (Institute of Physics, Tallin, Estonia) for his help with the instrumentation used for molecular beam spectroscopy and for many discussions. We thank Dr. J. Gauss and Prof. E. J. Heller (University of Washington, Seattle, WA) for their implementation of the wavepacket propagation algorithm. This work was made possible by a grant from the National Science Foundation (NSF CHE 91-06471).

Registry No. Pt(hfacac)$_2$, 65353-51-7.

(22) The formula to convert the dimensionless displacement Δ_i into ΔQ_i in angstroms is

$$\Delta Q_i = \left(6.023 \times 10^{23}\frac{\hbar}{2\pi c\omega m}\right)^{1/2}(10^8\Delta_i)$$

where m is the mass involved in the vibration in units of gram atomic weight (e.g. $C = 12$ g), ω is the wavenumber of the vibrational mode in cm^{-1}, $\hbar = h/2\pi$, where h is Planck's constant in g cm^2 s^{-1}, c is the speed of light in cm s^{-1}, ΔQ_i is the displacement in Å, and Δ is the dimensionless displacement.